

ATMOSPHERIC OPTICS

https://doi.org/10.1070/QEL17302

Peculiarities of adaptive phase correction of optical wave distortions under conditions of 'strong' intensity fluctuations

V.P. Lukin, N.N. Botygina, O.N. Emaleev, V.V. Lavrinov

Abstract. **The reason for the loss of efficiency of adaptive phase correction in the propagation of optical waves in a turbulent atmosphere under conditions of 'strong' intensity fluctuations is experimentally explained for the first time. Based on the data from experiments conducted on both horizontal and vertical atmospheric paths, we have found that intensity fluctuations begin to significantly affect phase measurements when the coherence radius of the optical wave becomes less than the radius of the first Fresnel zone. Under these conditions, the main meter of adaptive optics systems, i. e. the Hartmann sensor, no longer provides correct measurements of the phase distribution in the presence of deep amplitude modulation. Based on the study of the behaviour of the mode components of the phase fluctuations reconstructed from the results of measurements in various operating regimes, we have found that, first of all, the amplitudes of the lowest modes of phase fluctuation expansion (tilts, defocusing, and astigmatism) are distorted, which, as the analysis shows, is very different from the regime of weak fluctuations.**

Keywords: *adaptive phase correction, intensity fluctuations, tilts, defocusing, astigmatism, atmospheric turbulence.*

1. Introduction

The field of research related to the use of adaptive optics (AO) systems to improve the characteristics of optoelectronic systems operating in the atmosphere is currently being intensively developed. However, the effectiveness of such systems largely depends on the level of fluctuations in the parameters of optical waves caused by atmospheric turbulence. And this turns out associated with the manifestation of not only phase, but also amplitude fluctuations.

When analysing the efficiency of phase correction systems, it is usually assumed that there are no intensity fluctuations. In this case, the devices for phase measurements (interferometers, phase meters, etc.) operate most correctly. It is interesting to consider another limiting case – the presence of 'strong' intensity fluctuations, assuming that the adaptive system has an unlimited spatio-temporal resolution for correcting phase distortions. It is known that phase distortions acquired during the passage of a wave through an optically inhomogeneous medium transform into a modulation of the spatial intensity distribution as the wave propagates further. If the modulation is deep enough, the points with zero intensity may appear.

If an optical wave is described in terms of its complex amplitude U, then the points with zero intensity occur at the points of intersection (or tangency) of continuous lines on which the imaginary part vanishes. If $\mathrm{Re}U$ and $\mathrm{Im}U$ change their sign from positive to negative when intersecting these lines, such points are the points of wavefront dislocations. For adaptive phase correction, it is of importance that the appearance of dislocations violates the continuity of the two-dimensional phase distribution [1, 2]. When such discontinuities arise, the errors of the wavefront reconstruction and its approximation by an adaptive mirror using data of optical measurements increase significantly. In general, the use of special correctors also has no effect, since when correcting turbulent distortions, dislocations occur at randomly located points within the aperture. Algorithms for constructing the aberration map of the measured wave, currently used in most wavefront sensors (WFS's), give a continuous function of transverse coordinates. Herewith, they actually filter the vortex part of the measurement vector.

2. Numerical experiments

We will analyse the results of our numerical experiments [2–6], which indicate the impact of intensity fluctuations and phase distribution dislocations on the efficiency of turbulent distortion correction. Three aspects of this problem are of practical and scientific interest. The first aspect is how much the loss of amplitude information affects the efficiency of phase correction. The second aspect is how much the loss of information contained in the vortex part of phase measurements reduces the adaptation efficiency. And finally, the third aspect is the degree of effect of amplitude modulation on the data of phase measurements performed, for example, by a Shack–Hartman sensor. The latter circumstance seems to us the most important, since it makes it impossible to conduct direct phase measurements with significant amplitude fluctuations of the optical wave wavefront.

It should be noted that the first two aspects of the problem have been discussed in works [2–6]. In this case, numerical experiments were performed for two correction schemes operating both for the reception of radiation and for its propagation. The first scheme is a typical correction scheme for image reception. The second one is a correction scheme based on phase conjugation (PC) using data of phase measurements of the reference source.

When analysing the operation of these two schemes in [4–6], two variants of the phase measurement algorithm were

V.P. Lukin, N.N. Botygina, O.N. Emaleev, V.V. Lavrinov V.E. Zuev Institute of Atmospheric Optics, Siberian Branch, Russian Academy of Sciences, pl. Akad. Zueva 1, 634021 Tomsk, Russia; e-mail: lukin@iao.ru

Received 20 February 2020
Kvantovaya Elektronika **50** (9) 866–875 (2020)
Translated by M.A. Monastyrskiy

considered. The first one is an ideal adaptive system that instantly and accurately reproduces the reference wave phase over the entire cross-section plane, including singularities of the wave front (dislocations). In the second variant, only the component corresponding to the potential part of the vector field of local tilts of the wavefront is corrected. We call this correction a potential (or vortex-free) phase correction.

Thus, in fact, we have implemented [5, 6] four schemes of a numerical experiment, namely an ideal reception compensation system, a compensation system for only the potential part of phase aberrations, an ideal PC system, and a PC system for only the potential part of aberrations.

As shown in work [7], to analyse the problem of propagation of optical radiation along atmospheric paths, four parameters should be employed: the propagation path length L, the diameter D of the receiving system's aperture, the wavelength λ, and the turbulence intensity C_n^2. According to the similarity theory [7], the problem of plane wave propagation in a turbulent atmosphere is characterised by only two scales: the coherence radius r_0 can be chosen as the transverse scale, and the diffraction length for a beam with a radius equal to the coherence radius ($L_d = kr_0^2$) may serve as the longitudinal scale. Then the problem is characterised by the relative path length L/L_d and the relative aperture diameter D/r_0. In this case, the variance β_0^2 of intensity fluctuations (scintillation index) [7] calculated for a plane wave in the case of a power-law turbulence spectrum is uniquely associated with the ratio L/L_d: $\beta_0^2 = 2.9(L/L_d)^{5/6}$. Therefore, it can be used as a parameter instead of the L/L_d ratio.

The results of our numerical experiments [4–6] are shown in Figs 1 and 2. Figure 1 shows the dependences of the Strehl ratio SR on the scintillation index for the distortion compensation scheme. It is known that the Strehl ratio is numerically equal to the ratio of the average value of the axial intensity of an image formed in a turbulent medium to that of the system operating in vacuum.

For an ideal compensation scheme, the Strehl ratio SR is virtually independent of either the relative aperture diameter or the path length. The difference between the SR ratio and the value corresponding to the diffraction limit (SR = 1) is almost imperceptible. This is consistent with the idea that phase fluctuations play a major role in image distortion, while the role of amplitude fluctuations is insignificant. In this case, the phase fluctuations are completely corrected. In the case of ideal compensation only for the vortex-free part of the phase, the correction efficiency decreases quite significantly with an increase in the scintillation index. A twofold decrease in the SR ratio is achieved already at $\beta_0^2 \approx 1-1.5$. Further increase in the intensity fluctuations leads to the fact that the intensity at the lens focus tends to an uncorrected value. The correction efficiency decreases by an order of magnitude at $\beta_0^2 = 3$, i. e. at $L \approx L_d = kr_0^2$.

Similar results were obtained for the PC scheme. This means that the efficiency of this phase correction decreases (Fig. 2) when the path length reaches the diffraction length L_d. It turns out that the correction efficiency for an ideal PC scheme (Fig. 2) depends on the magnitude of intensity fluctuations. However, this dependence is not as strong as one might expect. At $\beta_0^2 = 3$, the SR ratio decreases to 0.8 and is almost independent of the aperture diameter.

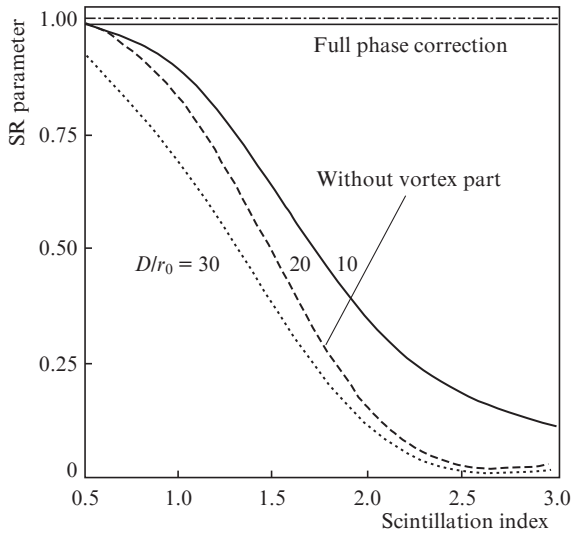

Figure 1. Dependences of the Strehl ratio SR on the scintillation index for the image correction scheme at different values of D/r_0.

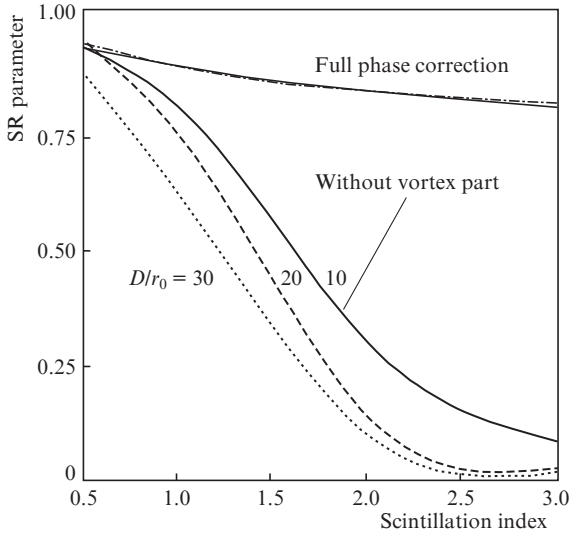

Figure 2. Same as in Fig. 1 for the PC scheme.

3. American experiment

Until recently, there was only a limited amount of experimental data that could be compared with the results of numerical analysis given in [5, 6]. There is a single known experiment conducted at MIT Lincoln Laboratory (USA) on an atmospheric horizontal path of 5.5 km [8]. The adaptive system included a Hartmann sensor and a deformable mirror. The problem of focusing the radiation beam was solved using the PC algorithm. The wavelengths of the reference and corrected beams were 633 and 514 nm, respectively.

Figure 3 shows an approximation obtained from calculations performed in [4–6] using the experimental data of Ref. [8]. From these data, it is difficult to judge to what extent the reduction in the correction efficiency is associated with phase discontinuity and filtration of phase dislocations, and to what extent it is due to other factors, such as an increase in the ratio of the aperture diameter to the coherence radius, the errors of the wavefront distortion sensor and the adaptive system. However, a good agreement with the results of our calcula-

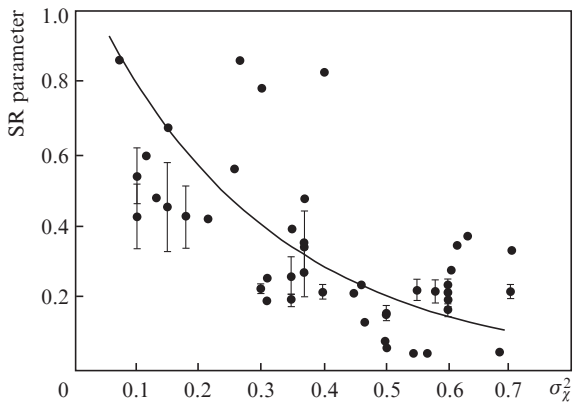

Figure 3. Dependence of the Strehl ratio SR on the variance of fluctuations of the amplitude's logarithm for a spherical wave, calculated by formula (2) from [5]: (points) experimental data [8] and (solid curve) their approximation.

tion suggests that mainly the use of the algorithm for reconstructing the reference beam wavefront, filtering the vortex phase, is the decisive factor determining the correction efficiency reduction.

4. Preliminary conclusions

Based on the said above and the results of works [2–6], we can formulate the following preliminary conclusions:

1. The proposed numerical model of the AO system, which includes a 'filtering' algorithm for the wavefront reconstruction, allows us to adequately model and quantify the adaptive correction efficiency under conditions of strong intensity fluctuations.

2. When correcting turbulent distortions, the PC system efficiency decreases by about half with an increase in the variance β_0^2 of intensity fluctuations (scintillation index) from zero to unity. In this range of β_0^2 values, the correction efficiency does not virtually depend on the ratio of the aperture diameter to the coherence radius. With a further increase in intensity fluctuations, the correction efficiency begins to depend on the aperture diameter. The increase in the β_0^2 value to 3 reduces the correction efficiency by an order of magnitude or more, and the SR ratio tends to the value obtained in the system without correction.

3. Since the variance value $\beta_0^2 = 3$ approximately corresponds to the limit of applicability of the smooth perturbation method (SPM) [7], it can be assumed that the SPM applicability violation is associated with the occurrence of wavefront dislocations. Note that the intensity vanishes at the points of dislocations, and the logarithm of the amplitude turns to infinity, while the SPM is actually a perturbation method for the logarithm of the field.

4. A decrease in the efficiency of the adaptive correction of the vortex-free phase with an increase in the variance of intensity fluctuations occurs in approximately the same way both in the phase compensation scheme and in the PC scheme.

It is interesting to note that even at large amplitude fluctuations, the use of adaptive phase correction still provides a certain and quite significant gain (in terms of the Strehl ratio) [6, 9] compared to the case without correction. Table 1 contains the ratios of the corrected SR_c parameter to its uncorrected SR_0 value for the vortex-free phase compensation scheme at the variance of $\beta_0^2 = 3$. It can be seen from Table 1 that for all values of D/r_0, the corrected value of the Strehl ratio is about four times greater than the uncorrected value.

Table 1. Relative gain in the Strehl ratio obtained when correcting only the potential phase.

D/r_0	SR_0	SR_c	SR_c/SR_0
10	0.0324	0.129	3.98
20	0.0106	0.038	3.58
30	0.0051	0.025	4.90

As we have shown earlier in [4–6], the greatest effect from the application of the phase correction system can be only obtained if certain conditions are met on the atmospheric path. In particular, a good adaptive correction is only possible for atmospheric paths whose length is less than the turbulent diffraction length, i.e., $L < L_d = kr_0^2$. This condition can be derived from the most natural condition, namely (see [5, 6, 9, 10]) from the fact that the effective operation of the AO system on an atmospheric path of length L is only possible if the isoplanatism angle, numerically equal to r_0/L, exceeds the angular resolution of the system:

$$r_0/L > \lambda/r_0. \tag{1}$$

Note that formula (1) deals with the coherence radius r_0 (Fried's radius) calculated for a short exposure [8]. It is easy to show that condition (1) matches the condition

$$r_0 > \sqrt{\lambda L}, \tag{2}$$

which, in turn, corresponds to the manifestation of weak intensity fluctuations on the path:

$$k^{7/6} C_n^2 L^{11/6} < 1. \tag{3}$$

It is in this case that adaptive systems using the PC algorithm are effective, and the Hartmann sensor gives correct phase data, since the impact of amplitude fluctuations in the system can be ignored.

On vertical paths, conditions (1)–(3) are almost always met, but on horizontal paths the situation easily changes to the opposite, i.e., the Fried coherence radius becomes less than the radius of the first Fresnel zone [which can be easily obtained from condition (1)]. This means that amplitude fluctuations begin to appear, and the variance of intensity fluctuations calculated from formula (3) becomes greater than unity. Under such conditions, the AO phase systems become inefficient, and it is no longer possible to achieve any improvement by using PC [5, 6, 9].

5. Experiments with strong fluctuations

It should be noted that the conclusions regarding a decrease in the efficiency of phase AO systems with an increase in the level of amplitude fluctuations were obtained by us in the course of numerical simulation. In this case, the main distorting factor was the inability to describe the phase front as a smooth surface, and the simulation was performed in the absence of noise. Under real conditions, in addition to the signal, the WFS is affected by all sorts of interferences and noises. This, in turn, causes the phase measurement data to become incor-

rect. The algorithms for the Shack–Hartmann sensor operation are protected to some extent from amplitude fluctuations due to the fact that, when evaluating the centre of gravity of the focal spot, the signal is normalised to the amount of the light flux through the subaperture. However, the requirements for improving the WFS accuracy necessitate the use of subapertures with a size smaller than the coherence radius, and this necessitates working with small subapertures when the level of amplitude fluctuations increases. At small subapertures, strong fluctuations in the light flux occur, which leads to the phase measurement errors.

In our experiments [11], we found the dependence of phase systems on the level of intensity fluctuations, which is manifested primarily in the WFS operation. The appearance of significant amplitude fluctuations leads to a change in the brightness (scintillation) of focal spots on the Hartmann matrix. In this case, the phase measurement results become incorrect.

There is a high level of fluctuations on horizontal atmospheric paths, while the sensors operate under conditions of high environmental variability, especially under urban conditions; seasonal changes and a strong dependence of the optical signal amplitude on the aerosol content in the atmosphere are also observed. Consequently, at real levels of turbulence under urban conditions, phase systems can only operate over limited distances.

To verify this statement, we performed numerous measurements between August 2017 and August 2018. Below are the results of analysis of experimental data obtained in recent years using the AO system prototype [11] both on extended vertical and horizontal atmospheric paths.

5.1. AO system prototype

To conduct experiments in the atmosphere, a prototype of the AO system was designed, in which a PC scheme with a reference source was implemented (Fig. 4). To form a reference source, we used the reflection of the light from an angle reflector illuminated by a semiconductor IR laser. This laser was located behind the secondary mirror of the telescope in its 'blind' zone. The beam from the reference source was directed to the atmospheric path through a forming device, which partially compensated for the large original angular divergence of the laser light. At the opposite end of the path, a special measuring test pattern was installed with an angle reflector mounted on it, which returned the light to the transmitter. The size of the reflective element of the angle reflector was varied by placing an opaque screen in front of the reflector. By varying the size of the open part of the angle reflector, it is possible to form the reflected light with both a plane wavefront and a wavefront that occurs in the case of a point reflector-scatterer. On paths up to 2.5 km long, a reflector less than 1 cm in size was used, which corresponds to the spherical wave approximation. Guidance of IR laser light on the reflector was carried out by observing the reflected signal on the prototypes video camera.

In Fig. 4, a MEADE astronomical telescope without an eyepiece, which we used in our experiments, is conventionally shown as a lens L1. Reflected reference IR light and light from the object (in the visible wavelength range) are fed to the input aperture of this telescope, and then, using an optical periscope formed by two plane mirrors, are transmitted to the upper platform, on which the main elements of the prototype are installed. Two lenses, L1 and L2, form the first scaling collimator designated to match the sizes of the telescope's input aperture and flexible mirror. On the upper platform, after two reflections from a plane rotating mirror and a flexible (deformable) mirror, the radiation enters the WFS input, in front of which a second scaling collimator is placed, indicated in the diagram as lenses L3 and L4. This collimator ensures that the sizes of the flexible mirror and the WFS analysis area are matched. In addition, a beam-

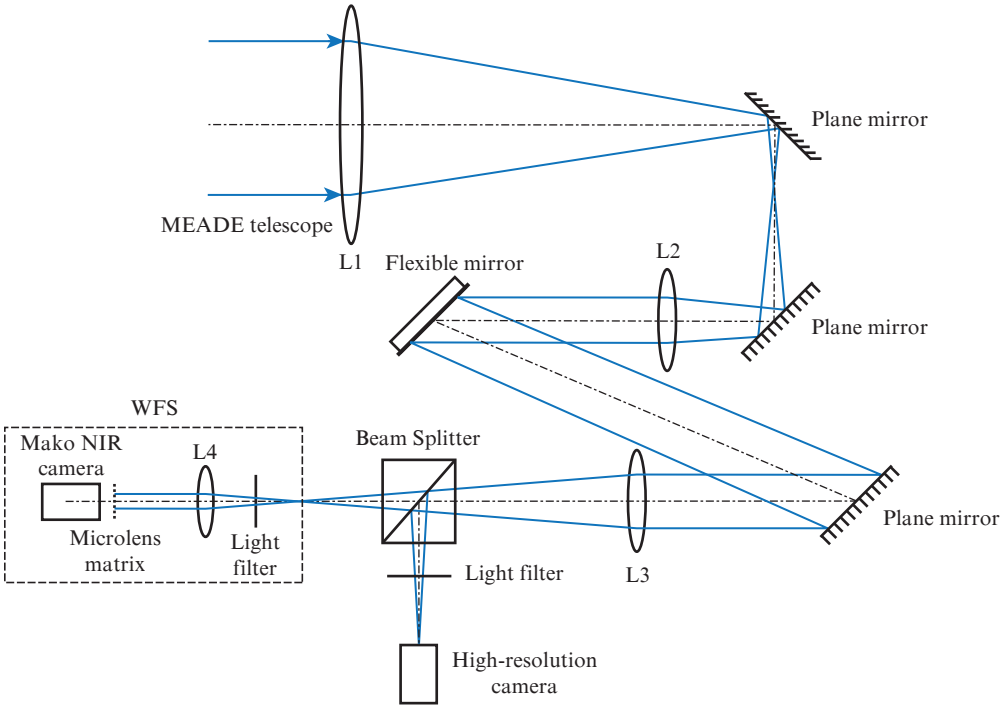

Figure 4. Prototype's optical scheme.

splitter is introduced into the scheme, which directs part of the corrected light to a high-resolution video camera. The separation of the visible and reference IR light in the receiving system is performed using two filters. One filter is installed in front of the WFS, while the second one is located directly in front of the high-resolution video camera.

Phase fluctuations in the reference wave along the atmospheric path were measured by a Shack–Hartman WFS. To close the feedback loop at the atmospheric path end, a measuring test pattern was installed as the test object of analysis, at the centre of which an angle reflector was placed, providing sufficient power of the reference light without the involvement of a high-power laser for illumination.

5.2. WFS parameters

Our prototype used a WFS implementation operating according to the Shack–Hartmann scheme. The sensor is based on a Mako G-223B NIR camera, which operates in the infrared range and serves to measure phase fluctuations using a reference source. At full resolution, this camera produces about 50 frames per second. The choice of camera is consistent with the choice of the reference source wavelength. The reference source's operating wavelength 0.808 μm is in one of the transparency windows of the Earth's atmosphere. In addition, telescope glasses have high transmittance at this wavelength.

To develop a WFS operating according to the Shack–Hartmann scheme, an element is needed that divides the receiving aperture into separate elements, the so-called subapertures. To this end, diffraction microrasters were used in the WFS optical scheme. These microlens rasters were calculated and manufactured using a unique technology developed at the Institute of Automation and Electrometry, SB RAS (Novosibirsk) [12]. These are diffractive optical elements. The prototype used two rasters with different numbers of elements in a matrix with square packing of elements: 10×10 and 18×18. This made it possible to operate the prototype under different turbulence conditions.

Table 2 shows the parameters of microrasters cut from glass in the form of circles with a diameter of 12 mm. The microrasters are mounted close to the focal plane of the receiving telescope directly in front of the Mako G-223B NIR camera, thus forming an ordered system of focal spots on the camera sensor. Therefore, all angular (or phase) distortions on the input pupil of the telescope lead to linear displacements of the centres of gravity of the system of focal spots formed through these microrasters. Calculations show that, even with a microraster of 10×10 subapertures, the developed WFS ensures wavefront reconstruction [11, 13, 14] and expanding it to at least the 35th Zernike polynomial.

Table 2. Parameters of microlens rasters.

Size	Period/μm	Focus/μm
10×10	518	51377
18×18	259	8500

The WFS operation was provided by a special program [13]. This program was used for computer data processing and calculation of the phase distortion distribution by converting the angular displacement matrix of the system of focal spots at the telescope's input aperture. Next, the expansion by Zernike polynomials of the phase distortions measured at the telescope's input aperture was constructed. As a result, the WFS-based measurements [11, 13] give the current values of the amplitudes of the mode components of phase fluctuations at the telescope's input aperture. Using the expansion of measurement data by orthogonal Zernike polynomials [14], a formula can be obtained for any mode component of phase fluctuations, which relates the variance of fluctuations of this mode component and Fried's radius. Further, this characteristic can be used to quantify image distortion.

Here we present the simplest calculation formulae for determining Fried's radius using WFS data. In doing so, we proceed from the assumption that the angle reflector generates a nearly spherical wave. This wave, having passed through the IR filter, is separated from the visible range light and forms a WFS signal. Fried's radius is calculated from the measurement data of the variance of the difference of random displacements (jitters) of two focal spots separated by a certain distance, which are formed by two subapertures. Using the well-known formula obtained in [15], which relates the variance $\Sigma(d)$ of the difference of random angular displacements with Fried's radius r_0, the receiving aperture diameter D, and the distance d between the subapertures, we obtain the expression for calculating Fried's radius:

$$\Sigma(d) = 2\sigma^2\left[1 - \frac{5}{9}(d/D)^{-1/3}\right], \tag{4}$$

where

$$\sigma^2 = 0.18\left(\frac{D}{r_0}\right)^{5/3}\left(\frac{\lambda}{D}\right)^2. \tag{5}$$

These simple relations allowed us to estimate Fried's radius directly from experimental data. In this case, the current measurement data of Fried's radius were averaged during the experiment. Based on the prototype parameters used, it is possible to estimate the smallest value of Fried's radius on the atmospheric path, measured using the WFS. It turned out to be about 2 cm. For such Fried's radius, the worst value of the viewing angle θ in a turbulent medium [7] is determined by the formula

$$\theta \approx 0.98\lambda/r_0 \tag{6}$$

and constitutes about 5″ for a wavelength of 0.55 μm.

The computer in the system's prototype was used both for calculating the coordinates of the centres of gravity of focal spots and the variance of the jitter difference, and for estimating Fried's radius according to formulae (4) and (5). Since our measurements were conducted at the reference wavelength of 0.808 μm, and the image formation in the system was performed in the visible region (at $\lambda = 0.555$ μm), the measurement data should be recalculated. According to calculations [5, 6, 9], the following formula can be used to recalculate the measurement data obtained for the wavelength λ_1 to the data for the wavelength λ_2:

$$r_0(\lambda_2) = (\lambda_2/\lambda_1)^{6/5} r_0(\lambda_1). \tag{7}$$

If the WFS operates at a reference wavelength of 0.808 μm, and the recalculation corresponds to the centre of the visible wavelength range, i.e., at $\lambda = 0.555$ μm, the recalculation factor is 0.64.

However, the matter is not limited to the requirement to recalculate Fried's radius. In addition, if the wavelengths of

the reference and fundamental radiation do not coincide, the image correction efficiency decreases. In our works [6, 9], it was shown that the use of a reference source at a wavelength different from the wavelength of the original radiation leads to a decrease in the correction efficiency, while the Strehl ratio begins to decrease. From these results, it follows that the most effective reference source is a source operating at the wavelength of fundamental radiation.

In the prototype, a flexible U-Flex-36-MDL-24 mirror is used for phase correction, which, thanks to its design [16], includes a special arrangement of control electrodes on a piezoelectric plate and thus makes it possible to form an optical surface with a complex relief and compensate for aberrations up to the 4th order (the degree of expansion by the Zernike polynomials [14]). Thus, this mirror, together with a multichannel system of amplifiers, can correct tilts, defocusing, astigmatism, coma, and 4th-order aberrations. And, as estimates show, such a mirror is ultimately capable of reducing the variance of residual phase fluctuations by about six to seven times [11, 15].

5.3. Revealed features of the operation of the AO system prototype

In recent years, quite a lot of publications have appeared on the operation of atmospheric systems on extended paths [17–22]. However, no analysis of the possibility of operation of such systems in the presence of strong intensity fluctuations has been conducted in these works.

Perhaps, in this regard, only the paper [21] should be singled out, which describes the AO system being developed for functioning within the city. It uses a telescope with an aperture of 127 mm. The work was carried out on a horizontal path up to 3 km long at a height of 10–12 m above the underlying surface. The AO phase system used a Hartman sensor with 21 subapertures, and the system operation was performed using a reference beacon in the visible spectrum region. In [21], it is stated that the results are not very good due to strong turbulence; in particular, it is noted that it is necessary to quadruple the measurement point density on the WFS. However, the authors of [21] did not even suggest that the real cause of poor correction could be the inability of the WFS to operate effectively.

In this regard, we first of all tried to analyse the limiting capabilities of the AO phase system prototype, proceeding from the parameters of the components involved. If the system is designed on the basis of a telescope with an aperture diameter of 356 mm, and the camera in the WFS provides a rate of about 50 Hz, then, with the number of subapertures in the raster of 18×18, the minimum measured value of Fried's radius can be 2 cm. The number of control zones in the U-Flex-36-MDL-24 flexible mirror is 24.

As a rule, on long horizontal atmospheric paths (in the visible wavelength range), already at a length of $\sim$1 km, the Fried coherence radius becomes less than the radius of the first Fresnel zone. This means that amplitude fluctuations begin to appear, and the variance of intensity fluctuations calculated by formula (2) turns out to be greater than unity. Under such conditions, the AO phase systems become inefficient, and it is no longer possible to achieve any improvement using phase correction. In some cases, the measured phase obtained outside the non-isoplanar region can only degrade the image quality.

Experimentally, the dependence of phase systems on the level of intensity fluctuations manifests itself primarily in a change in the brightness (scintillation) of focal spots in the Hartmann matrix. In this case, the phase measurements become incorrect. Consequently, under conditions of atmospheric turbulence on a 2-km-long path, the AO system can only operate effectively if the coherence radius exceeds 4 cm. Therefore, before starting to work with the phase correction system, it is necessary first to evaluate the coherence radius and only then decide whether the system can operate at such a distance. Always, if an adaptive correction system is used, the state of the atmosphere is studied in advance. For vertical paths, atmospheric turbulence models are used.

As an example, we demonstrate a fairly rapid change in the turbulence level that we found when working under urban conditions. The data of current measurements performed using the WFS at a distance of 2 km are shown in Fig. 5. These measurements were made in August 2018. It can be seen that although Fried's radius changes rapidly over time and its measured value is approximately 2.5 cm. It should be noted that due to the low frequency of the WFS camera (50 Hz), there are limitations on the prototype's operation speed. Thus, when using the traditional algorithm (fixed time-lag algorithm [23, 24]), the required minimum system's frequency can be calculated by the formula

$$f_c \approx \frac{v}{r_0^{5/6}} D^{-1/6}. \tag{8}$$

Here v is the transverse speed of the wind. Data from calculations performed using formula (8) show that on a 2-km-long path, the prototype parameters ensure efficient operation of the AO system with Fried's radius greater than 5 cm and a wind speed not exceeding 3.6 m s^{-1}. At higher wind speeds, only a partial correction will be observed.

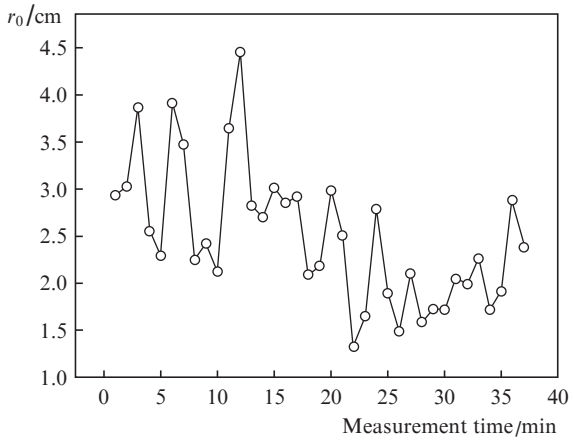

Figure 5. Estimate of the coherence radius for a spherical wave, obtained from differential measurements of the gravity centre's displacement of images formed by two vertically spaced WFS's. Measurements began at 7:20 am.

In our experiments (September–November 2017, May–July 2018), atmospheric parameters (wind speed and turbulence level) were being continuously measured using the METEO-2 meteorological system installed at the level of the system's receiving telescope. As the measurement data show, the overwhelming amount of measurements correspond to the turbulence level above 10^{-14} m$^{-2/3}$, while the wind speed is 2.5–4.5 m s^{-1}. At this turbulence level, there are indeed strong

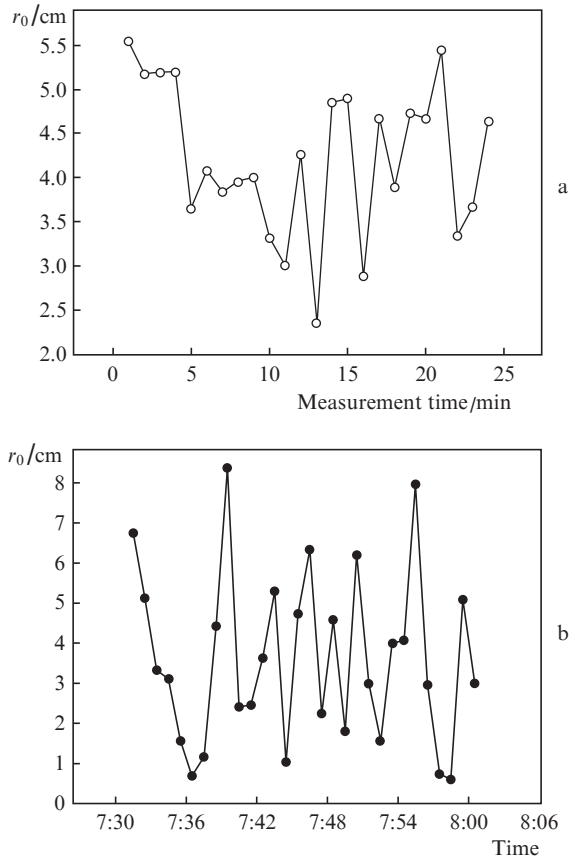

Figure 6. Estimate of the coherence radius for a spherical wave, obtained (a) from differential measurements of the gravity centre's displacement of images and (b) from measurements of the structural constant of the refractive index using the METEO-2 meteorological station (averaging time is 1 min). Measurements were performed on 18 July 2018; measurements began at 8:49 am.

fluctuations on the 2-km-long path. And only at a turbulence level of no more than 10^{-15} m$^{-2/3}$, the AO system will give a positive result under the additional condition of a weak wind. However, if the wind speed exceeds 3.6 m s^{-1}, or at smaller values of Fried's radius, the viewing quality may even deteriorate [11, 24].

It should be noted that atmospheric urban paths poorly yield to parametrisation, and it is difficult to construct local turbulence models for them. Therefore, the AO system development requires a preliminary stage of studying turbulence on the paths where the system will be operated. To this end, one can use both the WFS itself and the weather system installed on masts, on a helicopter or on a tethered balloon. In addition, information about the turbulence level and wind speed should be used when formulating system requirements.

Based on observations made in July 2018 using a prototype of the AO system prototype, we compared the behaviour of the measured mode components of phase distortions under weak and strong intensity fluctuations. The analysis results show that the appearance of intensity fluctuations leads to parasitic modulation of the lower-mode spectra and, consequently, causes a decrease in the phase correction efficiency. This primarily affects the data of phase measurements performed using the classical wavefront sensor, i.e. Shack–Hartmann WFS [11].

The measurements analysed further were made on a horizontal path up to 2 km long; the measurement time was the morning of July 18, 2018. A bank of fog or haze was observed on the optical path near the mira and the angle reflector. To estimate turbulent distortions, we used 3000-frame WFS data obtained with an image recording rate of 50 frames per second and a frame exposure time of 2 ms. When collecting data for subsequent processing, video frames were used in which the maximum illumination value of the images formed by each of the subapertures selected for measurements exceeded the background illumination by at least two times.

Our optical measurements made with WFS were accompanied by meteorological measurements with an acoustic meteorological station in the surface layer of the atmosphere (Fig. 6). These measurements showed that, in addition to the seasonal and daily variations, there was a rapid [11] variability (within a few minutes) in the turbulence intensity, causing a change in its integral value (cf. Figs 5 and 6a) even on extended horizontal paths. At the same time, when comparing Figs 5 and 6a with Fig. 6b, it should be taken into account that the meteorological data (Fig. 6b) correspond to measurements at a single point; therefore, it is impossible to talk of complete coincidence of the values. At the same time, it should be noted that changes occur synchronously, and the data are similar.

5.4. Wavefront aberration measurements

For optical phase measurements, the following parameters were used: frame rate, 50 Hz; frame exposure time, 2 ms; realisation duration, 10 s; radiation wavelength, 0.81 μm; angle reflector diameter, 7 mm; and path length, 2 km. The values of the structural constant of the refractive index, obtained using the METEO-2 meteorological station at 8:30:30 and 8:31:30 am are 5.87×10^{-15} m$^{-2/3}$ and 1.94×10^{-14} m$^{-2/3}$, and the coherence radii of a spherical wave propagating along the optical path are 5.9 and 2.9 cm, respectively. Figure 7 shows instantaneous intensity distributions (individual frames were recorded at different time moments) in the focal plane of the video camera sensor. Figure 7a presents a frame with the highest illumination of the entire input aperture of the telescope, where the extreme illumination values in the entire hartmannogram are at least four times higher than the background illumination. Figure 7b displays a frame in which the maximum illumination in all focal images is at least three times higher than the background value. In Fig. 7c, only the 92nd subaperture forms an image of the background illumination, in all other images the maximum illumination is at least 1.7 times higher than the background illumination. Figure 7d demonstrates a frame with the lowest illumination of the entire input aperture of the telescope; in this frame, already 17 subapertures form images with maximum illumination below the threshold. Here, the threshold illumination is 1.5 times higher than the background one.

To further study the effect of amplitude fluctuations on phase measurements, we analysed the accuracy of estimating the position of the centres of gravity of the focal patterns of the Hartmann sensor at various threshold illumination levels, up to illumination levels 1.5 times higher than the background value. To this end, the maximum illumination of images formed by each WFS subaperture was measured for a 10-second realisation recorded on July 18, 2018 at 10:34 am. The structural constant value of the refractive index measured by the meteorological station at 10:34:30 am is 4.86×10^{-15} m$^{-2/3}$, and the coherence radius of a spherical wave propagating

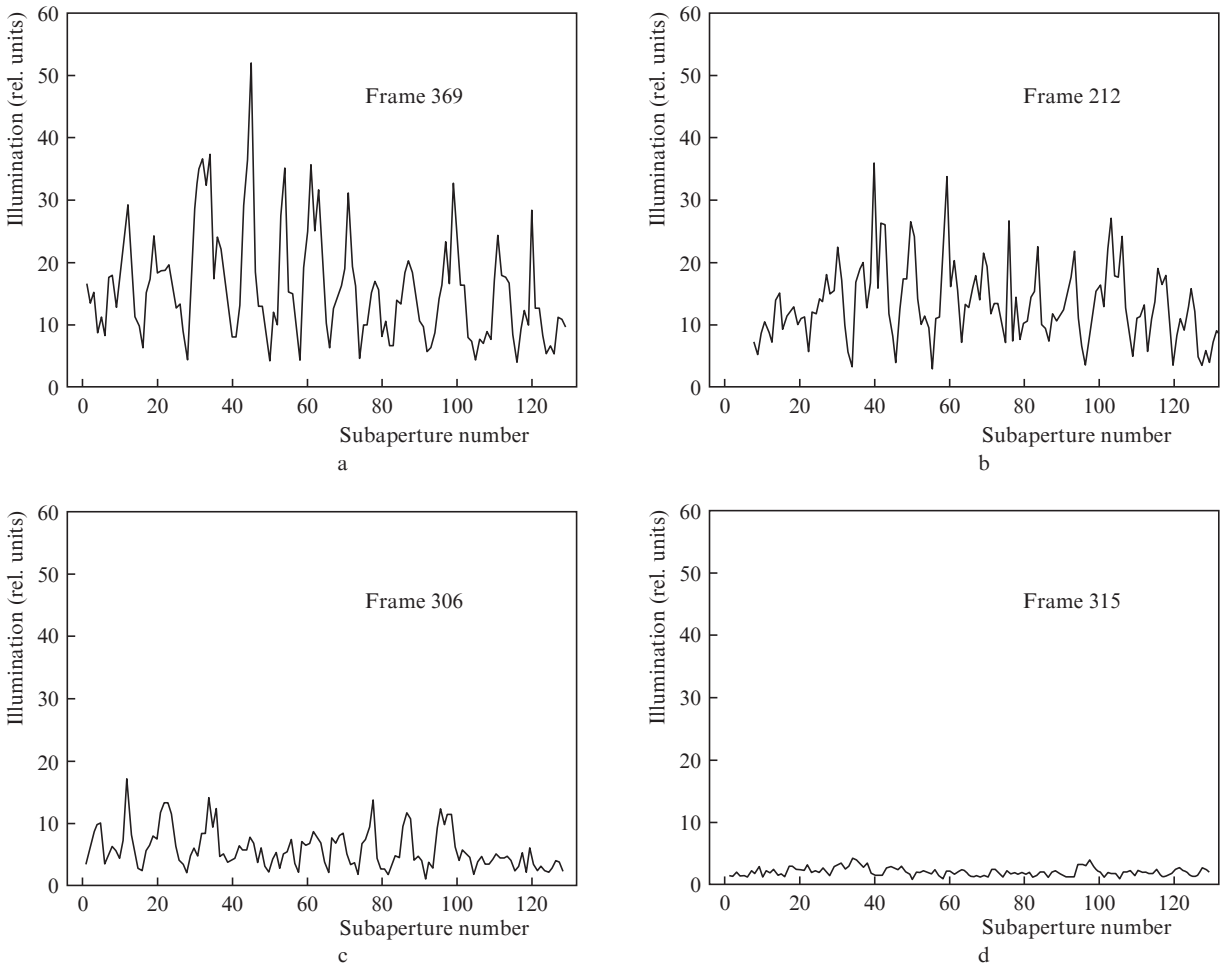

Figure 7. Maximum illumination values of images formed by each WFS subaperture, normalised to the background illumination.

along the optical path is 6.6 cm. Of course, as the amplitude of fluctuations increases, the error in estimating the position of local wavefront tilts increases. Then, based on the obtained video frames and using the developed program, the coefficients of the wavefront expansion by the main aberrations were calculated.

5.5. Expansion coefficients of wavefront aberrations

The data presented here were obtained from measurements made on July 18, 2018 starting at 8:31 am. From the measured realisations, the first 14 Zernike polynomials were calculated, starting from the wavefront tilts. Figure 8 shows only a part of the thus obtained data, namely the data for the first four Zernike polynomials with amplitudes C_1, C_2, C_3, and C_4.

Further, these data were used to calculate the corresponding spectra of mode expansions of phase fluctuations (Fig. 9). A decrease in the amplitude of the spectra by more than two orders of magnitude at frequencies above 15–20 Hz shows that the camera operation frequency (50 Hz) was quite sufficient to evaluate the main fluctuations. If we compare the spectra in Fig. 9 with the theoretical ones, calculated, for example, by R.J. Noll [14], we can see the irregularity of the spectra of the lowest mode components, which indicates their susceptibility to the action of amplitude fluctuations. This means that when amplitude fluctuations appear, the amplitudes of the lowest modes – wavefront tilts, defocusing, and astigmatism – are first distorted. At the same time, analysis shows that the higher modes numbered 7–14 remain virtually the same as in the case of weak intensity fluctuations.

The next step in the analysis of experimental data was to study the dependence of the pattern of focal spots on the level of amplitude fluctuations. Figure 10 shows the dependence of the number of subapertures, for which the illumination maximum is below the threshold (which does not allow the correct use of these subapertures in further analysis), on the frame number. It was also noted that in some frames, the illumination level of the pattern 'died away' almost to zero. Such frames cannot be used for wavefront reconstruction with acceptable quality, and they should be excluded from consideration.

In this regard, the next step in the development of phase reconstruction algorithms based on Shack–Hartman WFS data with adaptive control can be automatic discarding individual subapertures in the pattern obtained by the sensor, which will not be used for phase reconstruction. Then, only 'good' subapertures with the illumination exceeding the threshold value will be used in the calculation of phase fluctuations. In this case, of course, it is necessary to use a faster camera with the accumulation of a series of frames and averaging, while the phase reconstruction should be performed at the frequency value imposed by the presence of phase fluctuations. However, this can only be done if the signal level is sufficiently higher than the noise level. In addition, to combat the effect of amplitude fluctuations, multistage phase correc-

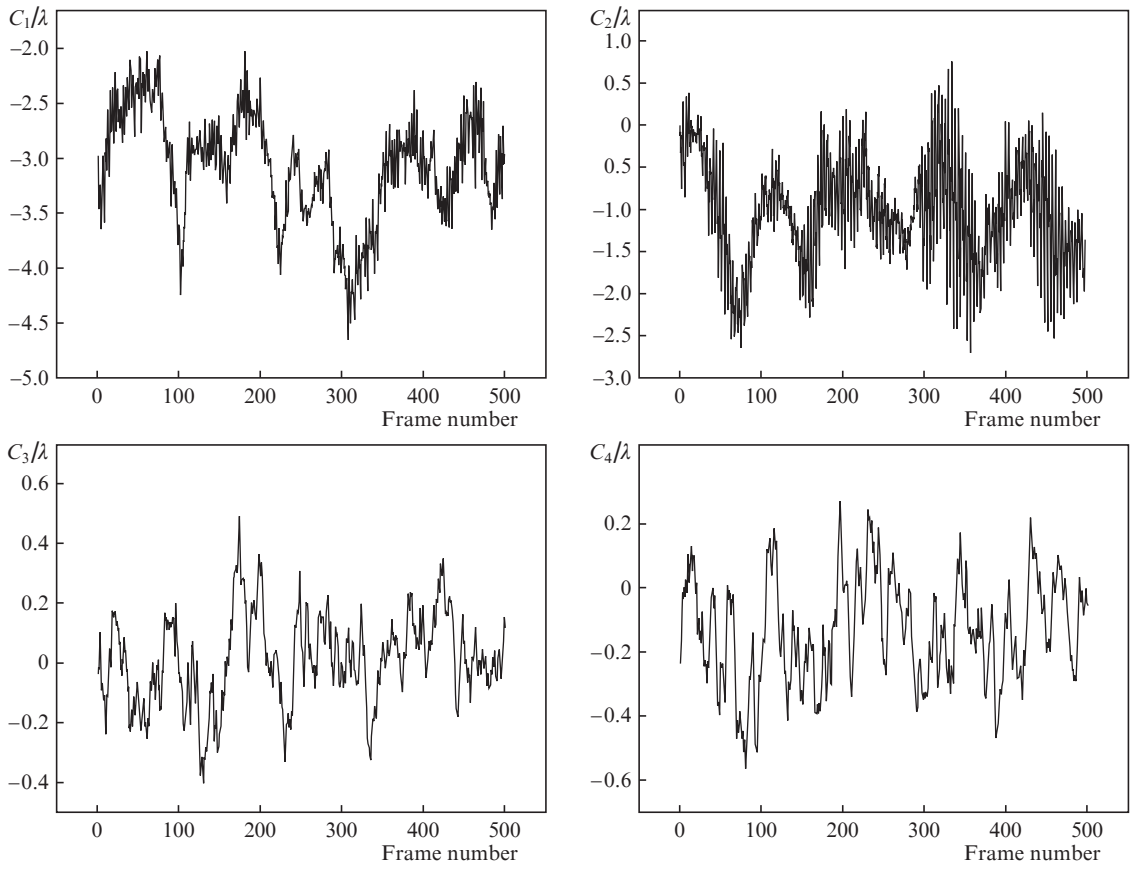

Figure 8. Expansion coefficients of the wavefront aberrations by Zernike polynomials.

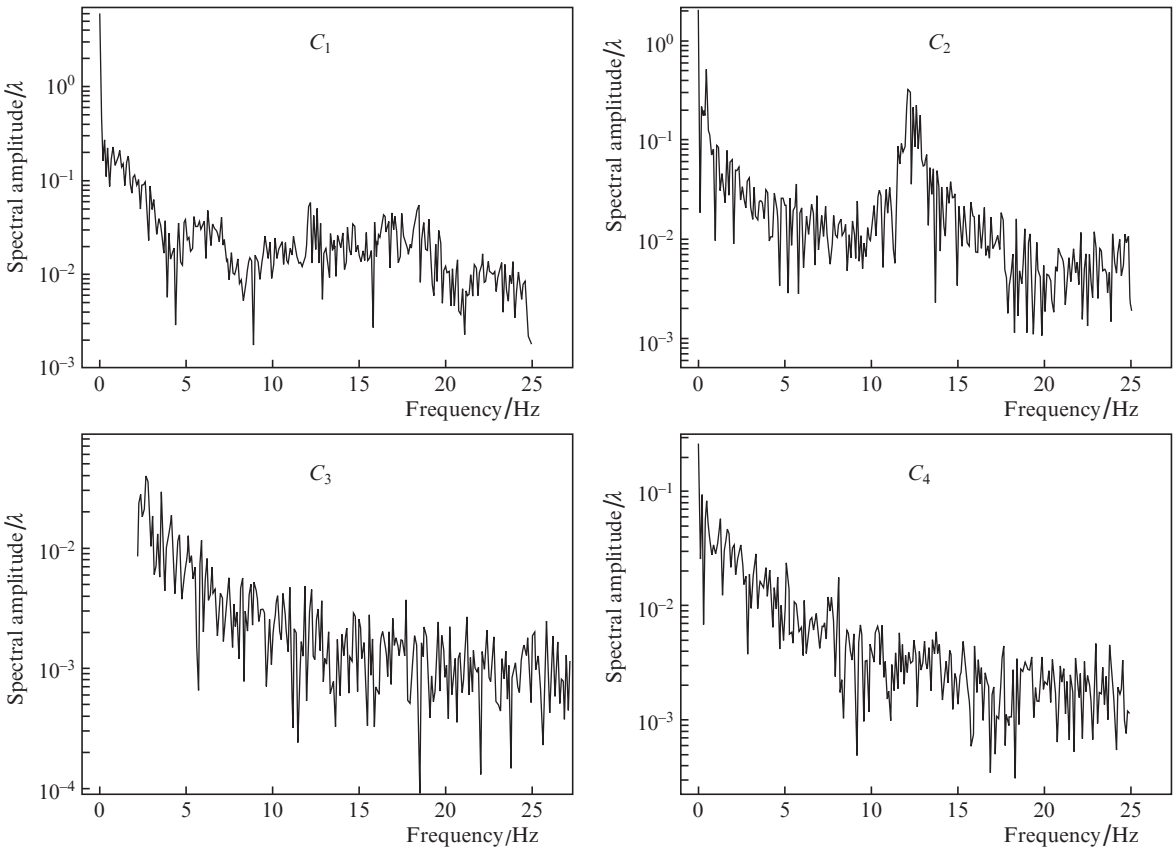

Figure 9. Amplitude spectra of the expansion coefficients of wavefront aberrations by Zernike polynomials.

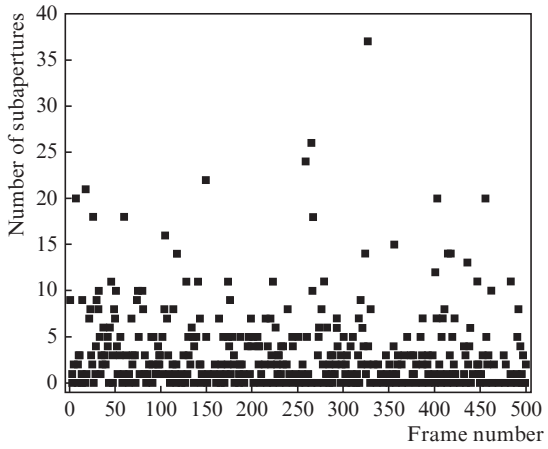

Figure 10. Number of subapertures that form images with maximum illumination below the threshold value (the illumination threshold is 1.5 times greater than the background one). Measurements were performed on 18 July 2018 at 10 : 34 am.

tion can be used along with non-phase sensors to measure fluctuations in the overall tilt and defocusing of the wavefront.

6. Conclusions

Based on the study of the behaviour of the mode components of phase fluctuations reconstructed from the results of measurements in various operating regimes, we have found that, as the level of amplitude fluctuations increases, the amplitudes of the lowest modes of the expansion of phase fluctuations – tilts, defocusing, and astigmatism – are first distorted, and the behaviour of these modes is very different from the classical behaviour corresponding to the regime of weak fluctuations. To overcome the impact of amplitude fluctuations, multistage phase correction can be used along with non-phase sensors to measure fluctuations in the overall tilt and defocusing of the wavefront.

Acknowledgements. The authors are grateful to A.A. Selin, E.L. Soin, and E.A. Kopylov for their help in setting-up the prototype and conducting experiments.

The work was performed with funding under Project II.10.3.5 'Development of methods and systems for adaptive correction for the formation of coherent beams and optical images in the atmosphere'.

References

1. Fortes B.V., Kanev F.Yu., Konyaev P.A., Lukin V.P. *J. Opt. Soc. Am. A*, **11** (2), 903 (1994).
2. Lukin V.P., Fortes B.V. *Proc. SPIE*, **3494**, 191 (1998).
3. Lukin V.P., Fortes B.V. *Opt. Atmos. Okeana*, **13** (5), 515 (2000).
4. Lukin V.P., Sennikov V.A., Tartakovski V.A. *Proc. SPIE*, **4338**, 57 (2000).
5. Lukin V.P., Fortes B.V. *Proc. SPIE*, **4034**, 176 (2000).
6. Lukin V.P., Fortes B.V. *Appl. Opt.*, **41** (27), 5616 (2002).
7. Gurvich A.S., Kon A.I., Mironov V.L. *Lazernoe izluchenie v turbulentnoi atmosfere* (Laser Radiation in a Turbulent Atmosphere) (Moscow: Nauka, 1976).
8. Primmerman C.A., Price T.R., Humphreys R.A., Zollars B.G., Barclay H.T., Herrmann J. *Appl. Opt.*, **34**, 2081 (1995).
9. Lukin V.P. *Quantum Electron.*, **35** (2), 143 (2005) [*Kvantovaya Elektron.*, **35** (2), 143 (2005)].
10. Vdovin G., Soloviev O., Loktev M., Savenko S. *Proc. SPIE*, **8178**, 81780F (2011).
11. Kopylov E.A., Lavrinov V.V., Lukin V.P., Selin A.A. *Proc. SPIE*, **10677**, 10677-65 (2018).
12. Koronkevich V.P., Poleshchuk A.G., Sedukhin A.G., Lenkova G.A. *Komp'yuternaya Optika*, **34** (1), 4 (2010).
13. Lavrinov V.V., Lavrinova L.N. Certificate of State Registration of Computer Programs No. 2018660752. Registration date: 28 August 2018.
14. Noll R.J. *J. Opt. Soc. Am.*, **66** (3), 207 (1976).
15. Lukin V.P., Nosov V.V. *Quantum Electron.*, **47** (6), 580 (2017) [*Kvantovaya Elektron.*, **47** (6), 580 (2017)].
16. DataSheet-DMU-36-MDL-24_a4_rus.pdf.
17. Kapranov V.V., Tugaenko V.Yu., Sukhareva N.A., Blank A.V., Babanin E.A. *Proc. XXIII Int. Symp. 'Optics of the Atmosphere and Ocean. Physics of the Atmosphere'* (Irkutsk: IAO SB RAS Publ., 2017).
18. Robert C., Fleury B., Michau V., Conan J.-M., Veyssiere L. Magli S., Vial L. *Proc. SPIE*, **6747**, 67470H (2007).
19. Marchi G., Weiß R. *Proc. SPIE*, **6747**, 67470I (2007).
20. Kasper M. *Proc. SPIE*, **8447**, 84470B (2012). DOI: 10.1117/12.924877.
21. Mackey R., Dainty Ch. *Proc. SPIE*, **7108**, 71080I (2008).
22. Jefferies St.M., Hope D.A., Hart M., James G. *Proc. SPIE*, **8890**, 88901C (2013).
23. Botygina N.N., Emaleev O.N., Lukin V.P. *Proc. SPIE*, **10425**, 22 (2017).
24. Lukin V.P., Sazonova P.V. *Izv. Vyssh. Uchebn. Zaved., Ser. Fiz.*, **59** (7), 121 (2016).